Hindawi
Advances in Civil Engineering
Volume 2018, Article ID 2076597, 7 pages
https://doi.org/10.1155/2018/2076597

Research Article

Effect of Thickness of Gravel Base and Asphalt Pavement on Road Deformation

Dongliang He[1,2] **and Weijun Yang**[1]

[1]*School of Civil Engineering, Changsha University of Science and Technology, Changsha, Hunan 410114, China*
[2]*School of Civil Engineering, Hunan University of City, Yiyang, Hunan 413000, China*

Correspondence should be addressed to Dongliang He; hedongliang14@126.com

Received 14 February 2018; Accepted 28 March 2018; Published 27 June 2018

Academic Editor: Rihong Cao

This study uses a test section of a highway, a study object, to explore the effect of thickness of the gravel base and asphalt layer on the vertical deformation of the road surface. The thickness of the asphalt layer and graded gravel base is changed. The nonlinear description equation of the relationship between the thickness ($h1$) of the asphalt layer and the vertical deformation ($d1$) is established: $d1 = a_4(1\ b_4^{h1})$. The thickness of the asphalt pavement is then determined to reduce vertical deformation. Numerical calculation shows that the maximum vertical deformation of the foundation is within 8 mm, which is less than the 15 mm maximum vertical deformation of the embankment. This level meets the design requirements.

1. Introduction

Semirigid base asphalt pavement is widely used as the main structure of highway pavements [1–3]. However, the widespread use of the semirigid base resulted in some problems, such as the short service life and reduced performance of the pavement, which will affect the safety of the highway [4–6]. The early destruction of the semirigid base asphalt pavement is affected by its structure [7–9]. Temperature and dry shrinkage tend to cause cracks on the semirigid base [10–12]. Zang et al. [13] developed a nondestructive FWD-based evaluation model to evaluate the semirigid base cracking condition. Wu et al. [14] simulated the interlayer bonding conditions between the semirigid base layer and the asphalt layer. Thus, rainwater easily enters from the pavement structure into the grassroots base and soil. This process is called subgrade softening, which causes early damage on the asphalt pavement. The particle material (graded gravel) between the asphalt surface layer and the semirigid base, which can be used as the stress dissipation layer, can effectively reduce the reflection crack of the semirigid material. Graded gravel is characterized by a certain degree of compaction of the medium material [15, 16]. Gravel particles can produce displacement and mutual dislocation and eventually achieve vibration compaction under the condition of traffic load vibration [17–19]. Volume compression in some gravel materials may cause the pore water pressure to rise due to dynamic loading, which decreases the material strength. Kuttah and Arvidsson [20] constructed a trial gravel road and exposed to various levels of the ground water table. Chang and Phantachang [21] investigated the effects of gravel content on the shearing characteristics of gravelly soils. The graded gravel base has good drainage performance. Thus, increased pore water pressure and decreased strength are not observed.

In this paper, the numerical simulation methods are used [22–26], which can simulate the construction of the road. A testing section of the Jiangxi Highway, China, is used as the engineering background to explore the effect of thickness of the bituminous pavement and the graded gravel base on the vertical deformation of the road surface. The thicknesses of the asphalt pavement and grading macadam base are changed. The vertical displacements are then studied.

2. Modeling and Parameters

2.1. Modeling. A section of a highway is selected for analysis (Figure 1). Given that most of road engineering embankments are symmetrical, the FLAC3D [27–31] is used for modeling analysis in half of the embankments, as shown in

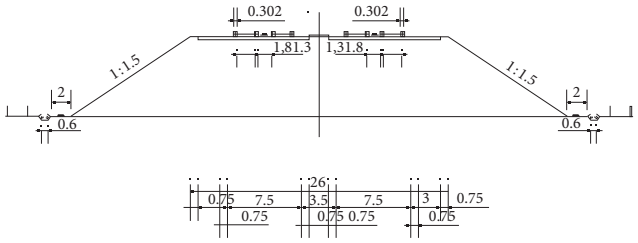

Figure 1: Calculation section.

Figure 2. The total height of the embankment is 8 m, and the slope is 1 : 1.5. The width of the embankment is 25 m, and the width of the upper road is 13 m. The foundation is equal to the height of the slope, which is 10 m, and the slope to the right is about 1 time the width of the embankment, which is 25 m. Table 1 shows the parameters of the embankment modeling according to the actual data provided by the project. For the gravel base, the Mohr–Coulomb criterion [32–34] is used to describe the stress and strain relation, the cohesion is 0.8 MPa, and the friction angle is 24°.

2.2. Calculation Scheme. The model range of the embankment is relatively large. The focus of the study is the vertical deformation of the embankment under road load. The action range is not large because the vehicle load force on the road of uniformly distributed load is 167 kPa. The vertical deformation of the pavement is largest in the pavement under load. Therefore, the main part of the study is the road surface. This study selects three kinds of pavement forms with different thicknesses of the asphalt layer and gravel layer. The main contents of analysis and parts of the embankment model are observed. The selection of the pavement and gravel thickness is based on three criteria (Figure 3): (1) the thickness of the asphalt pavement is 0.1 m and the gravel base thickness is 0.2 m, which is shortened to 10 to 20 types; (2) the thickness of the asphalt pavement is 0.18 m and the gravel base thickness is 0.2 m, which is shortened to 18 to 20 types; (3) the thickness of the asphalt pavement is 0.2 m and the gravel base thickness is 0.6 m, which is shortened to 20 to 60 types.

Vertical deformation is the vertical deformation of the pavement. The distance between the location and embankment center is given as follows:

his id 1 gp zdis 0.0 0.0 0.0
his id 2 gp zdis 2.0 0.0 0.0
his id 3 gp zdis 2.6 0.0 0.0
his id 4 gp zdis 2.7 0.0 0.0
his id 5 gp zdis 2.8 0.0 0.0
his id 6 gp zdis 2.9 0.0 0.0
his id 7 gp zdis 3.6 0.0 0.0
his id 8 gp zdis 4.7 0.0 0.0
his id 9 gp zdis 4.8 0.0 0.0
his id 10 gp zdis 4.9 0.0 0.0
his id 11 gp zdis 5.0 0.0 0.0
his id 12 gp zdis 5.7 0.0 0.0
his id 13 gp zdis 6.4 0.0 0.0
his id 14 gp zdis 6.5 0.0 0.0
his id 15 gp zdis 6.6 0.0 0.0
his id 16 gp zdis 6.7 0.0 0.0
his id 17 gp zdis 7.6 0.0 0.0
his id 18 gp zdis 8.5 0.0 0.0
his id 19 gp zdis 8.6 0.0 0.0
his id 20 gp zdis 8.7 0.0 0.0
his id 21 gp zdis 8.8 0.0 0.0
his id 22 gp zdis 9.5 0.0 0.0

History is divided into two parts, namely, wheel load and unacted part.

His id 1, 2, 7, 12, 17, and 22 are the unapplied load parts located in the middle of the load interval between the two wheels. The other part of his id is the part of the wheel load. Each wheel load has two edges and a total of four points in the center. His id 3, 4, 5, and 6 are the first group. His id 8, 9, 10, and 11 are the second group. His id 13, 14, 15, and 16 are the third group. His id 18, 19, 20, and 21 are the fourth group.

The maximum vertical deformation under load is analyzed in this study. The vertical deformation of different positions is compared, as shown in Figures 4–6. The four curves in the upper part are the vertical deformation curves of the embankments in the corresponding four sets of wheel loads. The other part shows the vertical deformation curve of the embankment with the unapplied load. The vertical deformation of the position under the direct action of vehicle load is the same as that in engineering practice. Therefore, the vertical deformation value of the four groups of load is analyzed as follows. For the 10 to 20 type, the vertical deformations of his id 3, 4, 5, and 6 are compared with those of his id 13, 14, 15, and 16. The vertical deformation of the two places was between 6 mm and 7 mm, and the difference was not significant. Results are consistent with the 18 to 20 type.

3. Results and Analysis

3.1. Influence of Asphalt Pavement Thickness on Embankment. To study the effect of asphalt pavement thickness on the vertical deformation of the embankment, the following data are divided into three categories in accordance with the thickness of the gravel layer, which is 20, 40, and 60 cm, respectively.

As shown in the calculation in Figure 7, the vertical deformation of the pavement increases gradually with the increase of the thickness of the asphalt layer set at 10, 15, 18, and 20 cm when the gravel base thickness is set at 20 cm. However, the slope of the curve decreases. Therefore, the increase of asphalt thickness decreases the influence of vertical deformation. In addition, the relationship between the thickness ($h1$) of the asphalt layer and the vertical deformation ($d1$) presents nonlinear characteristics. The relationship between the two is quantitatively described by the following equation through the data fitting method:

$$d1 = a_4\left(1 - b_4^{h1}\right), \tag{1}$$

where a_4 and b_4 are the undetermined coefficients.

The fitting correlation coefficient of the four groups is higher than 0.99, which indicates high correlation. The vertical deformation of the pavement in the corresponding points is small when the thickness of the asphalt layer is 10 cm. The relative difference of vertical deformation is comparatively small when the thickness sizes of the asphalt layer are 15, 18, and 20 cm. The overall vertical deformation trend of the road is large in the middle and small on both sides. The vertical deformation of the near embankment center is larger than that of the close shoulder. The maximum vertical deformation of the road is at approximately 4.7 m from the embankment center.

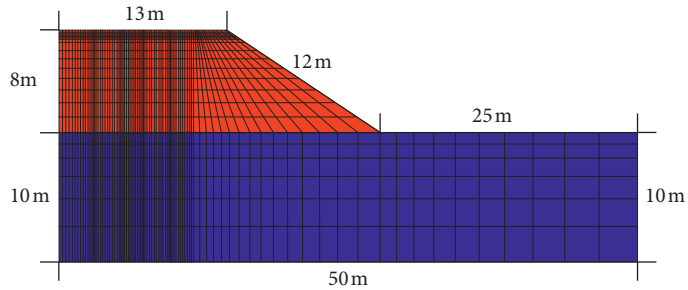

Figure 2: Model size in FLAC3D.

Table 1: Parameters for the embankment model.

Layer	Height (m)	Elastic modulus	Poisson's ratio	Constitutive model
Asphalt pavement	H1 = 0.1, 0.15, 0.18, and 0.2	1000 MPa	0.3	Elastic
Gravel base	H2 = 0.20, 0.40, and 0.60	—	—	Mohr–Coulomb
Embankment fill	H3 = 8 − H1 − H2	40 MPa	0.27	Elastic
Foundation	H4 = 10	40 MPa	0.27	Elastic

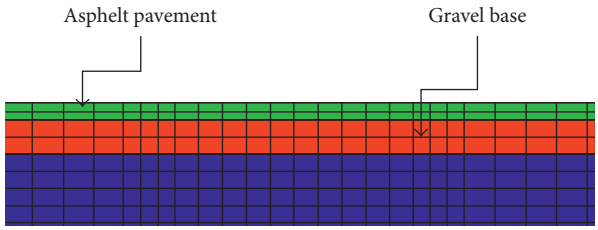

Figure 3: Road surface composition.

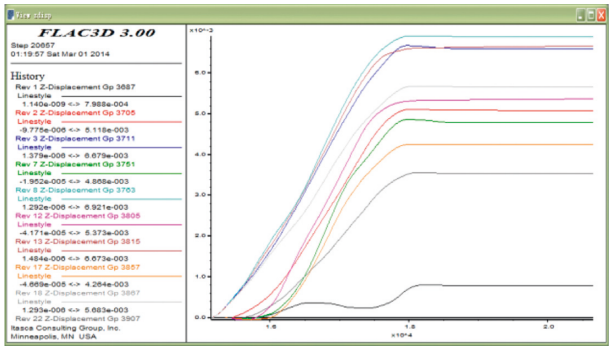

Figure 4: The vertical deformation for each history point of 10–20 type.

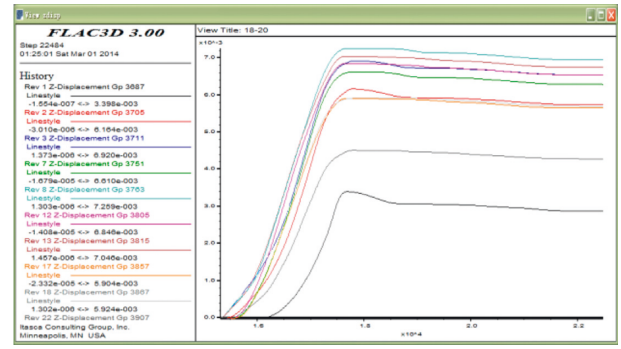

Figure 5: The vertical deformation for each history point of 18–20 type.

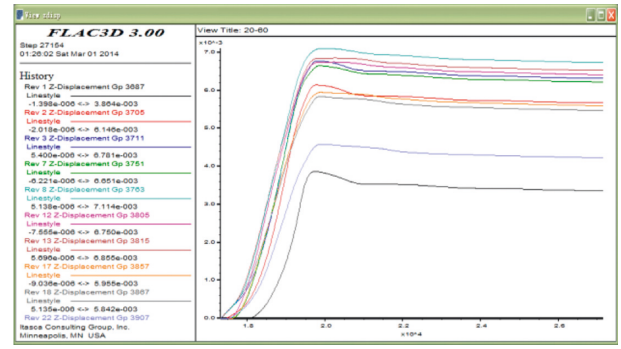

Figure 6: The vertical deformation for each history point of 20–60 type. (a) Thickness of the asphalt layer with 10 cm. (b) Thickness of the asphalt layer with 15 cm. (c) Thickness of the asphalt layer with 18 cm. (d) Thickness of the asphalt layer with 20 cm.

Previous analysis shows that vertical deformation of the pavement is the smallest of the four asphalt pavement thickness schemes when the thickness of the gravel layer is certain and the thickness of the asphalt pavement is 10 cm. In addition, the increase of the thickness of the asphalt layer does not significantly decrease the vertical deformation of the road pavement. To better understand the influence of asphalt pavement thickness on the vertical deformation of the pavement, this study analyzes the vertical deformation of the overall difference of the road surface (Figure 8). When the thickness of the asphalt surface is 10 cm, the vertical deformation of the pavement varies significantly from place to place although the maximum vertical deformation produced by the pavement is the smallest. The asphalt pavement cannot easily facilitate stress coordination. The relative vertical deformation of the pavement is large, and ruts develop easily, thereby destroying the asphalt pavement. The vertical deformation of the pavement decreased at asphalt pavement

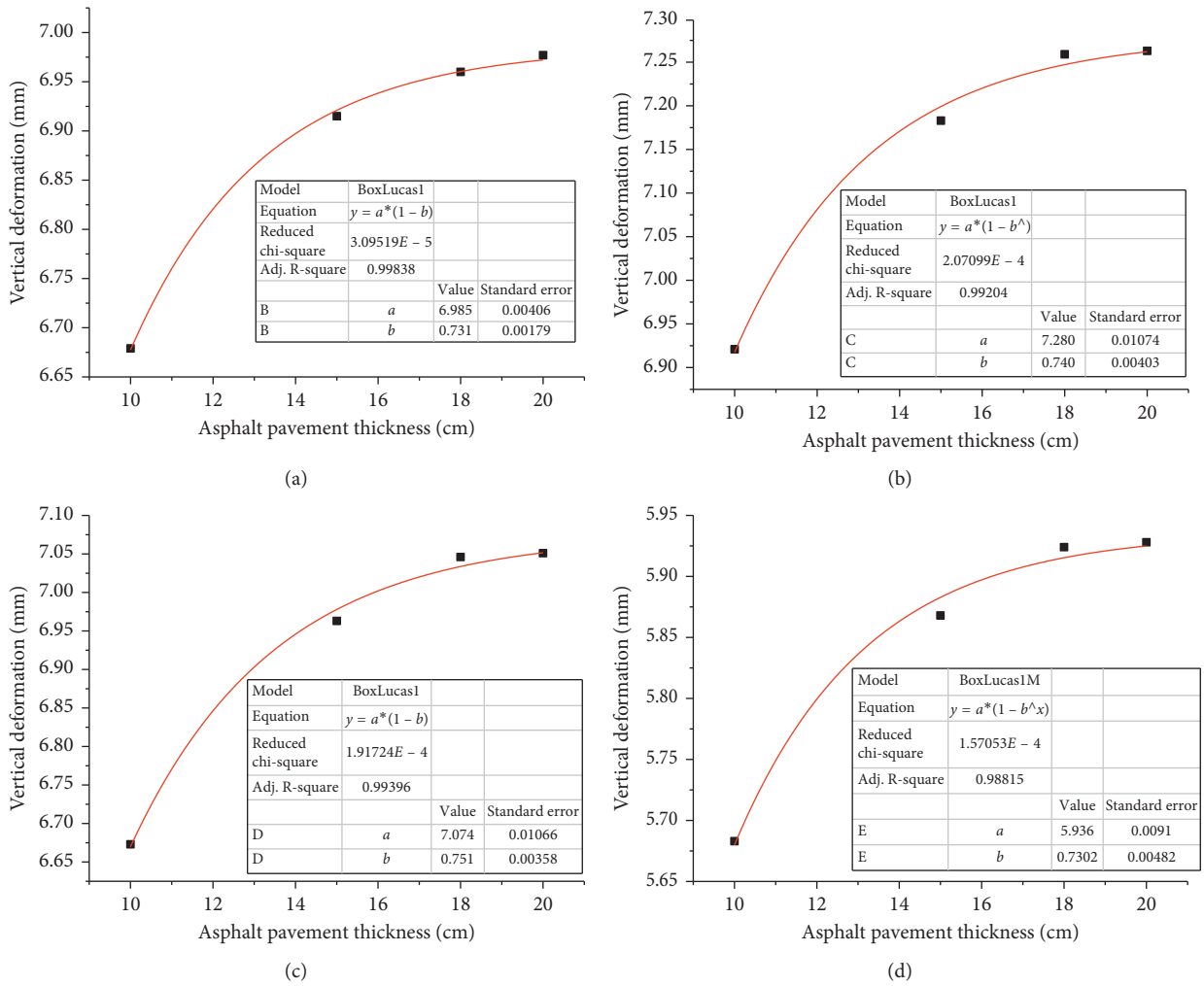

Figure 7: Vertical deformation of the road for 20 cm thickness of the gravel base.

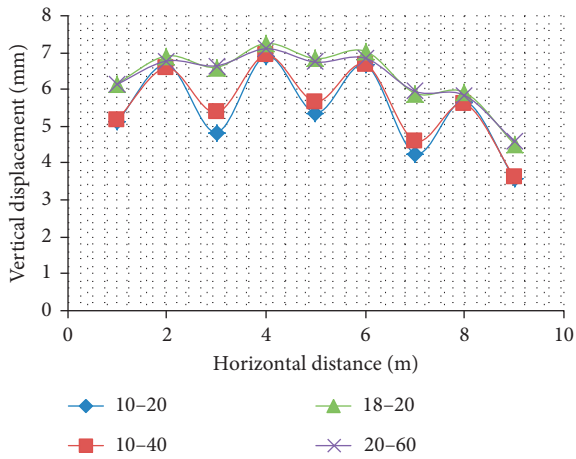

Figure 8: Relationship between the asphalt layer and pavement with uneven vertical deformation.

thicknesses of 10, 20, and 40 cm, but the effect is not significant. When the thickness of the asphalt surface is 18 or 20 cm, the maximum vertical deformation of the pavement is slightly increased, but the differences of the vertical deformation of the road are relatively small. The asphalt pavement coordinates the stress, while the relative vertical deformation of the pavement decreases. Compared with the vertical deformation of the asphalt pavement with thicknesses of 10, 18, and 20 cm, increasing the thickness of the asphalt pavement can significantly decrease the uneven vertical deformation of the pavement.

3.2. Influence of Gravel Base Thickness on Embankment. When the thickness of the asphalt pavement is 10 cm (Table 2), vertical deformation decreases on both sides of the road, and a trend of decrease after the first increase in the middle of the road is shown as the gravel base thicknesses of 20, 40, and 60 cm gradually increased. The vertical deformation of the pavement is smallest when the thickness of the gravel base is 60 cm, that is, when the gravel base is the thickest. The overall vertical deformation trend of the road is large and small on both sides. The vertical deformation of the near embankment center is larger than that of the close shoulder. The maximum vertical deformation of the road is

Table 2: Vertical deformation for the asphalt pavement thickness of 10 cm.

Thickness of the gravel base (cm)	First class	Second class	Third class	Fourth class
20	6.679	6.921	6.673	5.683
40	6.591	6.944	6.691	5.609
60	6.437	6.700	6.522	5.502

Table 3: Vertical deformation for the asphalt pavement thickness of 15 cm.

Thickness of the gravel base (cm)	First class	Second class	Third class	Fourth class
20	6.915	7.183	6.963	5.868
40	6.812	7.204	6.995	5.85
60	6.750	7.068	6.873	5.85

Table 4: Vertical deformation for the asphalt pavement thickness of 18 cm.

Thickness of the gravel base (cm)	First class	Second class	Third class	Fourth class
20	6.96	7.259	7.046	5.924
40	6.871	7.243	7.010	5.891
60	6.778	7.110	6.900	5.884

Table 5: Vertical deformation for the asphalt pavement thickness of 20 cm.

Thickness of the gravel base (cm)	First class	Second class	Third class	Fourth class
20	6.977	7.263	7.051	5.924
40	6.894	7.247	7.016	5.895
60	6.781	7.114	6.915	5.882

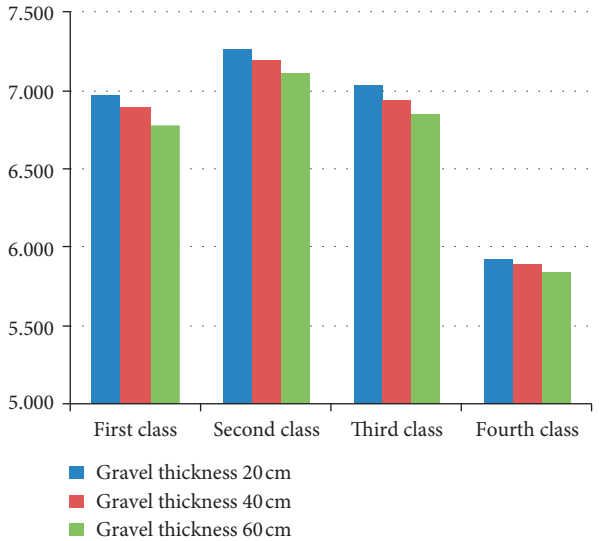

Figure 9: Vertical deformation for the asphalt pavement thickness of 20 cm.

at the direct part of the wheel load approximately 4.7 m from the embankment center.

When the thickness of the asphalt pavement is 15 cm (Table 3), the vertical deformation of the sides and the middle section decreases as the gravel base thicknesses of 20, 40, and 60 cm gradually increase, which is different from 10 cm thickness. The vertical deformation of the pavement in each group is smallest when the gravel base thickness is 60 cm, that is, when the gravel base is the thickest.

When the thickness of the asphalt pavement is 18 cm (Table 4), the vertical deformations on both sides of the road and of the middle two positions show a decreasing trend as the gravel base thicknesses of 20, 40, and 60 cm gradually increase.

When the thickness of the asphalt pavement is 20 cm (Table 5 and Figure 9), the vertical deformation caused by 20, 40, and 60 cm gravel base thicknesses is the same. Previous analysis shows that the increase of gravel base thickness can reduce the vertical deformation of the road when the thickness of the asphalt surface is certain. Therefore, the method of increasing the gravel base thickness can be used to reduce the vertical deformation of the road.

4. Conclusions

(1) The vertical deformation of the pavement increases as the thickness of the asphalt layer increases gradually from 10 cm to 15, 18, and 20 cm, but the slope of the curve gradually decreases.

(2) Asphalt pavement cannot easily facilitate stress coordination when the relative vertical deformation

of the pavement is large. Ruts may develop easily, thereby destroying the asphalt pavement. Compared with the vertical deformation of the asphalt pavement with thicknesses of 10 cm, 18 cm, and 20 cm, increasing the thickness of the asphalt pavement can significantly reduce the uneven vertical deformation of the pavement.

(3) When the thickness of the asphalt pavement is certain, the vertical deformation of the pavement decreases with the increase of the thickness of the gravel base from 20 cm, 40 cm, and 60 cm. The vertical deformation of the pavement in each group is smallest when the thickness of the gravel base is 60 cm.

Conflicts of Interest

The authors declare no conflicts of interest.

References

[1] M. Ameri, A. Mansourian, M. H. Khavas, M. R. M. Aliha, and M. R. Ayatollahi, "Cracked asphalt pavement under traffic loading–a 3D finite element analysis," *Engineering Fracture Mechanics*, vol. 78, no. 8, pp. 1817–1826, 2011.

[2] B. Huang, G. Li, D. Vukosavljevic, X. Shu, and B. K. Egan, "Laboratory investigation of mixing hot-mix asphalt with recycled asphalt pavement," *Transportation Research Record*, vol. 1929, pp. 37–45, 2005.

[3] M. A. Mull, K. Stuart, and A. Yehia, "Fracture resistance characterization of chemically modified crumb rubber asphalt pavement," *Journal of Materials Science*, vol. 37, no. 3, pp. 557–566, 2002.

[4] D. R. Roman, "A surrogate-assisted genetic algorithm for the selection and design of highway safety and travel time improvement project," *Safety Science*, vol. 108, pp. 305–315, 2018.

[5] S. Jung, K. Wang, C. Oh, and J. Chang, "Development of highway safety policies by discriminating freeway curve alignment features," *KSCE Journal of Civil Engineering*, pp. 1–9, 2017.

[6] J. Y. Rao, T. Xie, and Y. M. Liu, "Fuzzy evaluation model for in-service karst highway tunnel structural safety," *KSCE Journal of Civil Engineering*, vol. 20, no. 4, pp. 1242–1249, 2016.

[7] Q. Liu and D. Cao, "Research on material composition and performance of porous asphalt pavement," *Journal of Materials in Civil Engineering*, vol. 21, no. 4, pp. 135–140, 2009.

[8] K. L. Roja, A. Padmarekha, and J. M. Krishnan, "Influence of warm mix additive and loading rate on rutting of warm mix asphalt pavement," *International Journal of Pavement Engineering*, p. 16, 2017.

[9] E. V. Dave and B. Behnia, "Cohesive zone fracture modelling of asphalt pavements with applications to design of high-performance asphalt overlays," *International Journal of Pavement Engineering*, vol. 19, no. 3, pp. 1–19, 2017.

[10] M. Minhoto, J. Pais, P. Pereira, and L. Picado-Santos, "Predicting asphalt pavement temperature with a three-dimensional finite element method," *Transportation Research Record Journal of the Transportation Research Board*, vol. 1919, pp. 96–110, 2005.

[11] J. Qin and L. J. Sun, "Study on asphalt pavement temperature field distribution pattern," *Journal of Highway and Transportation Research and Development*, vol. 31, no. 4, 2006.

[12] S. M. Bazlamit and F. Reza, "Changes in asphalt pavement friction components and adjustment of skid number for temperature," *Journal of Transportation Engineering*, vol. 131, no. 6, pp. 470–476, 2005.

[13] G. Zang, L. Sun, Z. Chen, and L. Li, "A nondestructive evaluation method for semi-rigid base cracking condition of asphalt pavement," *Construction and Building Materials*, vol. 162, pp. 892–897, 2018.

[14] S. Wu, H. Chen, J. Zhang, and Z. Zhang, "Effects of interlayer bonding conditions between semi-rigid base layer and asphalt layer on mechanical responses of asphalt pavement structure," *International Journal of Pavement Research and Technology*, vol. 10, no. 3, pp. 274–281, 2017.

[15] J. Shaw and G. Gorrell, "Subglacially formed dunes with bimodal and graded gravel in the Trenton Drumlin Field, Ontario," *Geographie Physique et Quaternaire*, vol. 45, no. 1, p. 21, 1991.

[16] B. Yu, M. Zhang, and T. Li, "Analysis of the micro bonding graded gravel asphalt pavement structure," *Shenyang Jianzhu Daxue Xuebao*, vol. 29, pp. 852–860, 2013.

[17] J. E. Pizzuto, "The morphology of graded gravel rivers: a network perspective," *Geomorphology*, vol. 5, no. 3–5, pp. 457–474, 1992.

[18] K. G. Heays, H. Friedrich, B. W. Melville, and R. Nokes, "Quantifying the dynamic evolution of graded gravel beds using particle tracking velocimetry," *Journal of Hydraulic Engineering*, vol. 140, p. 04014027, 2014.

[19] D. P. Pham, Q. Su, W. H. Zhao, and A. T. Vu, "Dynamic characteristics and mud pumping mechanism of graded gravel under cyclic loading," *Electronic Journal of Geotechnical Engineering*, vol. 20, pp. 1391–1406, 2015.

[20] D. Kuttah and H. Arvidsson, "Effect of groundwater table rising on the performance of a Swedish-designed gravel road," *Transportation Geotechnics*, vol. 11, pp. 82–96, 2017.

[21] W.-J. Chang and T. Phantachang, "Effects of gravel content on shear resistance of gravelly soils," *Engineering Geology*, vol. 207, pp. 78–90, 2016.

[22] H. Lin, W. Xiong, and Q. Yan, "Three-dimensional effect of tensile strength in the standard Brazilian test considering contact length," *Geotechnical Testing Journal*, vol. 39, no. 1, pp. 137–143, 2016.

[23] M. Jiang, C. Sun, A. Rodriguezdono, N. Zhang, and J. Shao, "Influence of time-dependence on failure of echelon rock joints through a novel DEM model," *European Journal of Environmental and Civil Engineering*, vol. 19, no. 1, pp. s108–s118, 2015.

[24] I. Stefanou and J. Sulem, "Continuum modeling of discontinuous rock structures," *European Journal of Environmental and Civil Engineering*, vol. 14, no. 8-9, pp. 1199–1217, 2010.

[25] R. Cao, P. Cao, H. Lin, and X. Fan, "Experimental and numerical study of the failure process and energy mechanisms of rock-like materials containing cross un-persistent joints under uniaxial compression," *PLoS One*, vol. 12, no. 12, Article ID e0188646, 2017.

[26] A. T. Özer, O. Akay, and G. A. Fox, "A new method for remediation of sandy slopes susceptible to seepage flow using EPS-block geofoam," *Geotextiles and Geomembranes*, vol. 42, no. 2, pp. 166–180, 2014.

[27] H. Lin and J. Chen, "Back analysis method of homogeneous slope at critical state," *KSCE Journal of Civil Engineering*, vol. 21, no. 3, pp. 670–675, 2017.

[28] D. P. Zhu, Y. D. Lin, and E. Yan, "Three-dimensional numerical analysis on excavation and support of deep pit near the subway tunnel by computer simulation technique,"

Journal of Theoretical and Applied Information Technology, vol. 45, pp. 621–626, 2012.

[29] L. Z. Wu and R. Q. Huang, "Calculation of the internal forces and numerical simulation of the anchor frame beam strengthening expansive soil slope," *Geotechnical and Geological Engineering*, vol. 26, no. 5, pp. 493–502, 2008.

[30] M. Cai, P. Kaiser, H. Morioka et al., "FLAC/PFC coupled numerical simulation of AE in large-scale underground excavations," *International Journal of Rock Mechanics and Mining Sciences*, vol. 44, no. 4, pp. 550–564, 2007.

[31] M. C. He, J. L. Feng, and X. M. Sun, "Stability evaluation and optimal excavated design of rock slope at Antaibao open pit coal mine, China," *International Journal of Rock Mechanics and Mining Sciences*, vol. 45, no. 3, pp. 289–302, 2008.

[32] Y. Zhao, Y. Wang, W. Wang, W. Wan, and J. Tang, "Modeling of non-linear rheological behavior of hard rock using triaxial rheological experiment," *International Journal of Rock Mechanics and Mining Sciences*, vol. 93, pp. 66–75, 2017.

[33] A. Amavasai, J. P. Gras, N. Sivasithamparam, M. Karstunen, and J. Dijkstra, "Towards consistent numerical analyses of embankments on soft soils," *European Journal of Environmental and Civil Engineering*, pp. 1–19, 2017.

[34] J. F. Zou, S. S. Li, Y. Xu, H. C. Dan, and L. H. Zhao, "Theoretical solutions for a circular opening in an elastic–brittle–plastic rock mass incorporating the out-of-plane stress and seepage force," *KSCE Journal of Civil Engineering*, vol. 20, no. 2, pp. 687–701, 2016.